EINDHOVEN UNIVERSITY OF TECHNOLOGY

Full characterization of multiphase, multimorphological kinetics in flow-induced crystallization of IPP at elevated pressure

Citation for published version (APA):
Troisi, E. M., Caelers, H. J. M., & Peters, G. W. M. (2017). Full characterization of multiphase, multimorphological kinetics in flow-induced crystallization of IPP at elevated pressure. *Macromolecules*, *50*(10), 3868–3882. https://doi.org/10.1021/acs.macromol.7b00595

Document license:
CC BY-NC-ND

DOI:
10.1021/acs.macromol.7b00595

Document status and date:
Published: 23/05/2017

Document Version:
Publisher's PDF, also known as Version of Record (includes final page, issue and volume numbers)

Please check the document version of this publication:

• A submitted manuscript is the version of the article upon submission and before peer-review. There can be important differences between the submitted version and the official published version of record. People interested in the research are advised to contact the author for the final version of the publication, or visit the DOI to the publisher's website.
• The final author version and the galley proof are versions of the publication after peer review.
• The final published version features the final layout of the paper including the volume, issue and page numbers.

Link to publication

General rights
Copyright and moral rights for the publications made accessible in the public portal are retained by the authors and/or other copyright owners and it is a condition of accessing publications that users recognise and abide by the legal requirements associated with these rights.

• Users may download and print one copy of any publication from the public portal for the purpose of private study or research.
• You may not further distribute the material or use it for any profit-making activity or commercial gain
• You may freely distribute the URL identifying the publication in the public portal.

If the publication is distributed under the terms of Article 25fa of the Dutch Copyright Act, indicated by the "Taverne" license above, please follow below link for the End User Agreement:

www.tue.nl/taverne

Take down policy
If you believe that this document breaches copyright please contact us at:

openaccess@tue.nl

providing details and we will investigate your claim.

Download date: 04. Oct. 2023

This is an open access article published under a Creative Commons Non-Commercial No Derivative Works (CC-BY-NC-ND) Attribution License, which permits copying and redistribution of the article, and creation of adaptations, all for non-commercial purposes.

Macromolecules

Article

pubs.acs.org/Macromolecules

Full Characterization of Multiphase, Multimorphological Kinetics in Flow-Induced Crystallization of IPP at Elevated Pressure

E. M. Troisi,[†,‡] H. J. M. Caelers,[†] and G. W. M. Peters*[,†,‡]

[†]Department of Mechanical Engineering, Materials Technology Institute, Eindhoven University of Technology, P.O. Box 513, 5600 MB Eindhoven, The Netherlands

[‡]Dutch Polymer Institute (DPI), P.O. Box 902, 5600 AX Eindhoven, The Netherlands

Supporting Information

ABSTRACT: Understanding the complex crystallization behavior of isotactic polypropylene (iPP) in conditions comparable to those found in polymer processing, where the polymer melt experiences a combination of high shear rates and elevated pressures, is key for modeling and therefore predicting the final structure and properties of iPP products. Coupling a unique experimental setup, capable to apply wall shear rates similar to those experienced during processing and carefully control the pressure before and after flow is imposed, with in situ X-ray scattering and diffraction techniques (SAXS and WAXD) at fast acquisition rates (up to 30 Hz), a well-defined series of *short-term flow* experiments are carried out using 16 different combinations of wall shear rates (ranging from 110 to 440 s^{-1}) and pressures (100−400 bar). A complete overview on the kinetics of structure development during and after flow is presented. Information about shish formation and growth of α-phase parents lamellae from the shish backbones is extracted from SAXS; the overall apparent crystallinity evolution, amounts of different phases (α, β, and γ), and morphologies developing in the shear layer (parent and daughter lamellae both in α and γ phase) are fully quantified from the analysis of WAXD data. Both flow rate and pressure were found to have a significant influence on the nucleation and the growth process of oriented and isotropic structures. Flow affects shish formation and the growth of α-parents; pressure acts on relaxation times, enhancing the effect of flow, and (mainly) on the growth rate of γ-phase. The remarkably high amount of γ-lamellae found in the oriented layer strongly indicates the nucleation of γ directly from the shish backbone. All the observations were conceptually in agreement with the flow-induced crystallization model framework developed in our group and represent a unique and valuable data set that will be used to further validate and implement our numerical modeling, filling the gap for quantitatively modeling crystallization during complicated processing operations like injection molding.

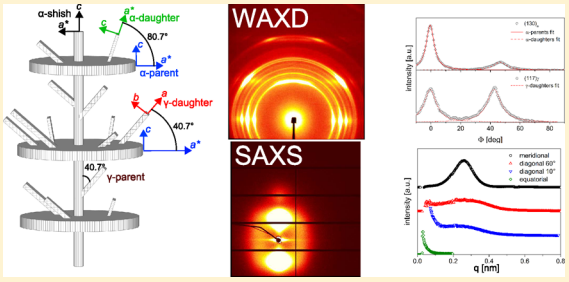

1. INTRODUCTION

Solidification of semicrystalline polymers in industrial processes is a complex matter: prior to and during crystallization, polymer melts experience steep thermal gradients, high deformation rates, and elevated pressure. These factors, and most often combinations of these, play a major role in affecting both crystallization kinetics and final morphologies and, consequently, the ultimate structure and properties.[1]

Among all the processing techniques, injection-molding, one of the most common industrial production processes to shape plastic parts, represents the most dramatic example: going from the walls to the center of the product, a distinctive skin−core structure is observed,[2,3] consisting of a quenched layer due to rapid cooling at the mold walls, a highly anisotropic shear-layer containing shish-kebab structures (crystalline morphology composed of a fibrous backbone with lamellar overgrowth), a fine-grained layer with low crystal orientation and high nucleation density, and an isotropic core crystallizing at elevated pressure.

The level of complexity increases when dealing with polymers which exhibit polymorphism, i.e., the ability to exist in more than one crystal form. Focusing on isotactic polypropylene, subject of this study, three different crystal forms (α, β, and γ) and a mesophase can all be found in injection-molded products.[2,4−8] Typically, the quenched layer is composed of mesophase due to the high cooling rates experienced, α and γ phase, promoted respectively by molecular orientation and elevated pressure, can simultaneously be present in the shear layer and in the isotropic core, whereas β mostly develops in the transition region between the shear and the fine-grained layers, nucleating from oriented flow-induced α-phase row nuclei. If conditions are such that elevated pressures are experienced during the injection and packing stage, complex morphologies can be found within the shear layer. The well-known shish-kebab structure consisting of an extended chain core crystal (shish) nucleating disk-like folded crystals (kebabs) can show epitaxial growth of both α and γ

Received: March 22, 2017
Revised: May 4, 2017
Published: May 12, 2017

 © 2017 American Chemical Society

DOI: 10.1021/acs.macromol.7b00595
Macromolecules 2017, 50, 3868−3882

lamellae (called daughters) from the kebab (in this case called parents) [010] lateral surfaces.[9,10]

In order to optimize processing techniques, as well as tune morphologies and crystal phases to achieve tailored products, it is vital to get understanding of the kinetics and mechanisms behind structure development in extreme conditions of flow and pressure.

During the past decades, several studies have been carried out, especially on the effect of shear flow on structure development, using different setups: sandwich-type shear cell,[11] Linkam shear cell,[12,13] pressure-driven flow cell,[14−16] and slit flow.[10,17] Most of the experiments were performed using the well-known *short-term flow protocol* introduced by the pioneering work performed in the group of Janeschitz-Kriegl.[18] Using this technique, the effect of flow on nucleation and orientation, at fairly low undercoolings, is separated from crystal growth analyzing the subsequent isothermal crystallization kinetics employing several in situ experimental techniques, like birefringence and X-ray techniques (SAXS, WAXD). Although this approach has been proved to be very valuable for the understanding of the structure formation in the early stage of flow, the experimental conditions are still very far away from real-life processing for semicrystalline polymers. Moreover, the experiments were performed at atmospheric pressure, whereas it is well-known that during injection-molding pressure represents an important factor that cannot be neglected.

The large majority of the work on the effect of pressure on crystallization of polymers has been performed using isobaric experiments using dilatometry techniques. It is well acknowledged that both nucleation densities and growth rates are influenced by pressure due to the shift of the equilibrium melting temperature upon pressurization. Focusing on iPP only, the complex polymorphism is affected: γ-phase grows in competition with α-phase and, at elevated pressure and temperature, becomes the only polymorph present above 170 °C and 2000 bar.[19−21]

Very little research has been performed on the combined effect of flow and pressure on the crystallization behavior of iPP, mostly due to the demanding experimental equipment able to apply flow at elevated pressure. Using an unique flow-device/dilatometer capable to work at pressure up to 1200 bar and shear rate of 180 s^{-1},[22] our group set foot in this field, providing an exclusive set of experimental data of iPP crystallized at elevated pressure after imposing strong shear flow. Van Erp et al.[23,24] found that shear flow does not act directly on the formation mechanism of γ-crystals but makes the crystallization to occur at high temperatures, which promotes γ-phase due to its higher growth rate at high temperatures. The fascinating morphology comprising shish kebabs with densely branched γ-daughters lamellae was observed for the combination of high pressure and high shear rates.[9] Differently, Yang et al.,[25] using a custom-designed pressuring and shearing device, observed suppression of γ-phase formation already at very low shear rates (3−9 s^{-1}) and high pressure (1000−1500 bar). This seeming discrepancy with our observation can be explained by the fact that the experiments were done using very long shear times (120 s): keeping the molecular orientation during crystallization prevents the material to crystallize in γ polymorph because of the peculiar not-parallel chain orientation in γ-crystals.[26,27] In all the research mentioned, sample characterization was performed post-mortem (measuring amount of crystal phases and orientation), with little insight into the dynamics of the structure development.

Using the outcome of van Erp experiments, Roozemond et al. developed a numerical model able to predict the results including the multiphase multimorphological kinetics, proposing some intersting concepts on the structural evolution, like an increased growth rate for the α-parent during and after flow due to residual molecular orientation and the growth of γ lamellae directly from the shish backbone.[28]

To close the circle on this complicated and fascinating topic and to validate Roozemond's crystallization model, we collected, for the first time, online experimental results during flow-induced crystallization of iPP at elevated pressure using in situ X-ray scattering and diffraction techniques (SAXS and WAXD) coupled with a modified slit-flow rheometer, able to control the pressure level before and immediately after flow. A fully characterized iPP, already employed in several other studies, was chosen as a model material. The kinetics of formation of different morphologies and crystal phases is fully quantified, and the key concepts driving flow-induced crystallization at elevated pressure are discussed and conceptually in agreement with our previous observations and modeling approach. This experimental data set will permit to validate and, if required, extend our multiphase, multimorphological crystallization model and, in the near future, be included in 2D finite element simulation, bringing us one step forward toward prediction of the complicated structure and morphology found in injection-molded products of iPP.

2. EXPERIMENTAL SECTION

2.1. Material. An isotactic polypropylene (iPP, Borealis HD601CF) with a weight-average molecular weight M_w of 365 kg/mol and a polydispersity index M_w/M_n of 5.4 is used in this work. A full characterization of the crystallization behavior of the same material has been performed in our group during the past decade.[28−30]

2.2. Methods. *2.2.1. Slit Flow Device.* Flow-induced crystallization (FIC) behavior under different pressure conditions was studied performing controlled shear experiments in a confined slit geometry (see Figure 1) within a modified multipass rheometer.[31] The slit dimensions are $w \times h \times L = 6 \times 1.5 \times 115$ mm. This unique device

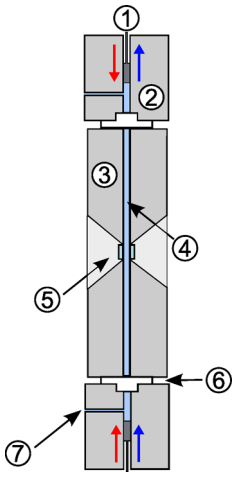

Figure 1. Schematic of the slit flow device employed in this study: (1) servo-hydraulically driven piston, (2) heated barrel, (3) flow cell, (4) polymer specimen, (5) X-ray observation window, (6) insulating ceramic ring, and (7) pressure transducer. The red and blue arrows show the directions of the movement of the two pistons during pressurization and shear flow, respectively.

DOI: 10.1021/acs.macromol.7b00595
Macromolecules 2017, 50, 3868−3882

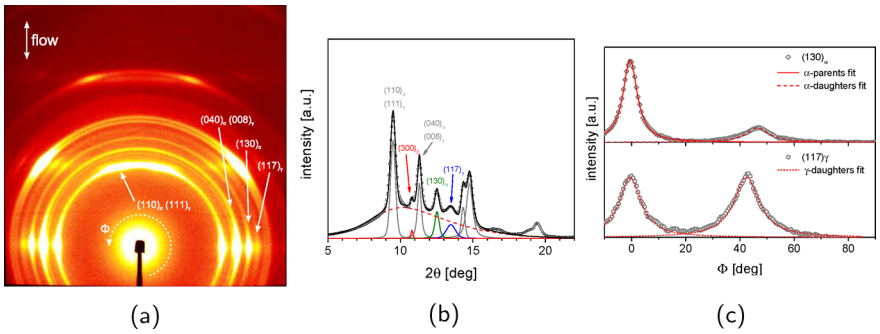

Figure 2. (a) 2D WAXD pattern collected at the end of the isothermal crystallization at 400 bar after being sheared for 0.25 s (v_{piston} = 80 mm/s). (b) Total integrated intensity as a function of the scattering angle (round markers), the dashed red line the amorphous contribution, and the black full line the fitting after deconvolution. (c) Azimuthal distributions of the $(130)_\alpha$ and $(117)_\gamma$ reflections; the red lines represent the fitting of the equatorial and off-axis maxima using Lorentzian functions.

allows to obtain high wall shear rates, comparable to the ones experienced during industrial injection-molding process, and to carefully control the pressure before and immediately after flow.

Pressure is applied by moving the two servo-hydraulically driven rectangular pistons (with the same cross-section dimensions as the slit), between which the polymer melt is confined, toward each others, and controlled by mean of two pressure transducers placed near each piston. Shear flow is imposed to the undercooled polymer melt by simultaneously moving the two pistons at the same time, in the same direction, with constant velocity. Cooling of the flow cell to the isothermal flow temperature is achieved by pumping a cooling medium through the cell (resulting in an average cooling rate of ≈7 °C/min and isothermal conditions within ±1 °C), while the temperature in the barrels, where the pistons are situated, is kept constant at a higher value to permit the proper functioning of the pressure transducers. The material rheology during flow is probed by measuring the pressure drop between the two transducers and a diamond window placed in the middle of the slit allows for online X-ray scattering measurements (Figure 1).

Prior to each experiment, the sample was molten at 220 °C for 10 min to erase any previous thermomechanical history and subsequently cooled down to the isothermal flow temperature, T^{flow}, of 145 °C. At this temperature the sample was pressurized to different pressures, P^{flow}, ranging from 100 to 400 bar. Once temperature and pressure were stable at the set values of T^{flow} and P^{flow}, shear flow was applied using four different piston speeds (20, 40, 60, and 80 mm/s) for a fixed time of 0.25 s. Within 0.5 s after shear flow was terminated the pressure reached 80% of the initial value of P^{flow}.

2.2.2. In Situ X-ray Measurements. Real-time small-angle X-ray scattering and wide-angle X-ray diffraction (SAXS and WAXD) measurements were carried out at beamline BM26B[32] at the European Synchrotron Radiation Facility (ESRF, Grenoble, FR) with a wavelength λ = 1.033 Å and a beam diameter of 300 μm.

Simultaneous acquisition of SAXS and WAXD patterns was performed using a Pilatus 1M detector (981 × 1043 pixels of 172 μm × 172 μm placed at a distance of 6.468 m) and a Pilatus 300 K detector (1472 × 195 pixels of 172 μm × 172 μm placed at a distance of 0.238 m), respectively. The detectors were triggered by an electric TTL pulse at the beginning of the pistons displacement. The first 3.96 s, from the start of flow, were monitored at an acquisition rate of 30 frames/s; the following 1200 s of isothermal crystallization were recorded using an acquisition time of 4 s. The Pilatus 300K detector has a limited azimuthal range, not sufficient to capture the complex orientation of different phases observed during in FIC of iPP under elevated pressures.[9] Therefore, WAXD experiments were repeated using a Frelon2K detector (2048 × 2048 pixels of 48.8 μm × 48.8 μm distance of 0.148 m). In this case an exposure time of 0.1 s for the first 4 s after flow and an exposure time of 4 s for the subsequent isothermal crystallization were used, resulting in a total acquisition time (exposure + readout) of 0.338 and 4.24 s, respectively.

The distance and tilt angle of the detectors were calibrated using AgBe (silver behenate) and α-Al_2O_3 (α-aluminum oxide) as standards for SAXS and WAXD, respectively. All X-ray images were first normalized for synchrotron beam fluctuations using an ionization chamber placed before the sample and for the transmission of the sample using a photodiode placed on the beamstop; subsequently, the background due to the air and empty cell scattering was carefully subtracted. In addition, 2D SAXS and WAXD patterns of a completely molten sample at T^{flow} and P^{flow} were collected and used as isotropic amorphous scattering patterns.

Finally, 2D SAXS and WAXD images were reduced to 1D intensity profiles as a function of the scattering angle (2θ) for WAXD and of the scattering vector ($q = (4\pi/\lambda) \sin \theta$) for SAXS using the software package FIT2D. Using the same software, azimuthal intensity distributions of characteristic WAXD reflection ($(130)_\alpha$ and $(117)_\gamma$) were obtained integrating the 2D pattern in a narrow 2θ range centered around the diffraction peak along the azimuthal angle (ϕ).

2.2.3. Wide-Angle X-ray Diffraction Data Analysis. A representative 2D WAXD pattern and the related 1D integrated intensity vs 2θ angle, collected at the end of isothermal crystallization for the experiment performed at 400 bar and 145 °C after shear using a piston speed of 80 mm/s (wall shear rate of 440 s^{-1}, see section 3.2) for 0.25 s, are shown in Figures 2a and 2b, respectively. The presence of the characteristics $(130)_\alpha$, $(300)_\beta$, and $(117)_\gamma$ reflections, centered at $2\theta \simeq$ 12.55°, 10.8°, and 13.5°, respectively, confirms the coexistence of α-, β-, and γ-phase crystals.

The azimuthal distributions of the $(130)_\alpha$ and $(117)_\gamma$ reflections, shown in Figure 2c, are in agreement with the previously reported morphology,[9,33−35] comprising α-"parents" lamellae with their c-axis parallel to flow/deformation direction and epitaxially grown γ- and α-"daughters" lamellae. The α-"daughters" branch at an angle of ∼80° and present their a-axis parallel to flow direction, whereas the γ-lamellae branch at ∼40° both from α-parents and shish backbone, with chain orientation parallel to flow direction. Our analysis does not allow to distinguish between γ-lamellae branching from the shish backbones and from the α-parents, since these have the same orientation. In the following, we will speak mostly in terms of γ-daughters but this does not mean that γ-lamellae nucleating from the shish backbones (γ-parents) do not exist; on the contrary, experimental observation from van Erp et al.[9] and modeling work by Roozemend et al.[28] showed that the high amount of γ-phase found in samples crystallized at high pressure after shear flow can be explained by the existence of γ-parents. In section 3.4.4 we will come back on this issue in more detail. A schematic of the morphology is given in Figure 3.

The apparent crystallinity evolution (apparent since it is an average over the slit thickness, because the X-ray beam traverses across the velocity gradient direction) was calculated after deconvolution of the total intensity scattered by the crystalline ($A_{crystal}$) and amorphous ($A_{amorphous}$) regions using

DOI: 10.1021/acs.macromol.7b00595
Macromolecules 2017, 50, 3868−3882

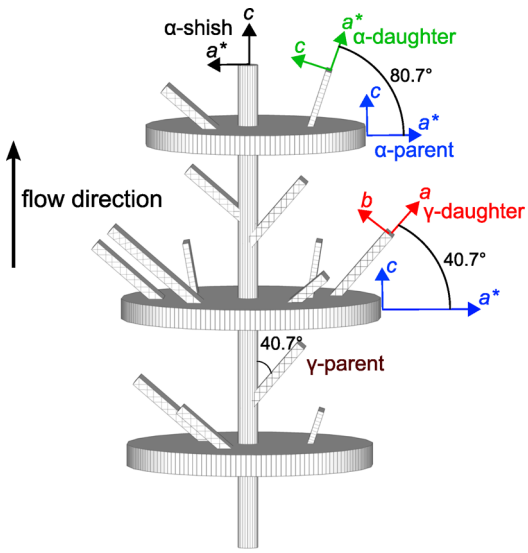

Figure 3. Schematic of the morphology of shish-kebab structure containing α- and γ-"parents" and α- and γ-"daughters" lamellae.

$$X_c = \frac{A_{crystal}}{A_{crystal} + A_{amorphous}} \times 100 \quad (1)$$

The apparent relative amount of crystals in the three different phases (α, β, and γ) was evaluated from the time-resolved X-ray diffraction profiles, as suggested by Turner-Jones et al.[36] and Murthy et al.,[37] by fitting the diffraction contribution due to the crystals using seven pseudo-Voigt funtions, as shown in Figure 2b. Measuring the area underneath the $(130)_\alpha$, the $(300)_\beta$, and the $(117)_\gamma$ reflections ($A_{130\alpha}$, $A_{300\beta}$, and $A_{117\gamma}$, respectively), the fraction of the each polymorph is given by the ratios

$$f_i = \frac{A_i}{A_{130\alpha} + A_{300\beta} + A_{117\gamma}} \quad i = \alpha, \beta, \gamma \quad (2)$$

The time evolutions of the different morphologies (α-"parents", γ-"daughters", and α-"daughters") are obtained by fitting of Lorentzian functions to the azimuthal distributions of the $(130)_\alpha$ and $(117)_\gamma$ intensities after subtraction of the amorphous and isotropic crystals contribution (if present) to the scattering (example in Figure 2c). For the $(130)_\alpha$ reflection, the area of the peak centered at the equator (ϕ = 0°) is representative of the amount of α-"parents" lamellae, whereas the area of the off-axis peak, centered at $\phi \sim 46°$, quantifies the amount of α-"daughters". For the $(117)_\gamma$ reflection, the area underneath both peaks, centered at $\phi \sim 0°$ (equator) and ~42° (off-axis), is proportional to the amount of γ-"daughters" lamellae.

2.2.4. Small-Angle X-ray Scattering Data Analysis. Figure 4a shows a representative 2D SAXS pattern of an iPP sample crystallized for 20 min at 400 bar after shear with a piston speed of 80 mm/s (same conditions of the WAXD pattern shown in Figure 2a). The two typical features of a shish-kebab superstructure can be easily recognized: a strong equatorial streak in the azimuthal region centered at ϕ = 0°, related to the scattering of the shish backbones aligned along the flow direction, and a well-defined meridional (ϕ = 90°) lobe due to the scattering of crystal lamellae (kebabs) oriented with their normal parallel to flow direction. As already observed by van Erp et al.,[9] the SAXS pattern shows also two additional features: a diffuse scattering in the azimuthal region defined at ϕ = 10° and a more clear correlation peak at ϕ = 60°. This observation, coherent with the already discussed WAXD features, confirms the existence of an oriented morphology including α-"parents", α-"daughters", and γ-"daughters" (see Figure 3).

As expected, the equatorial integrated intensity presented in Figure 4b (green diamond markers) does not show any correlation peak in the accessible q range (>0.029 nm^{-1}), indicating a very large correlation distance between shish (≫210 nm). Differently, three different maxima in intensity for the three other regions (meridional, diagonal 60°, and diagonal 10°) are observed, corresponding to three different spacings ($L_b = 2\pi/q^*$ = 22.9, 17.5, and 20 nm) between α-"parents", γ-"daughters", and α-"daughters" lamellae, respectively.

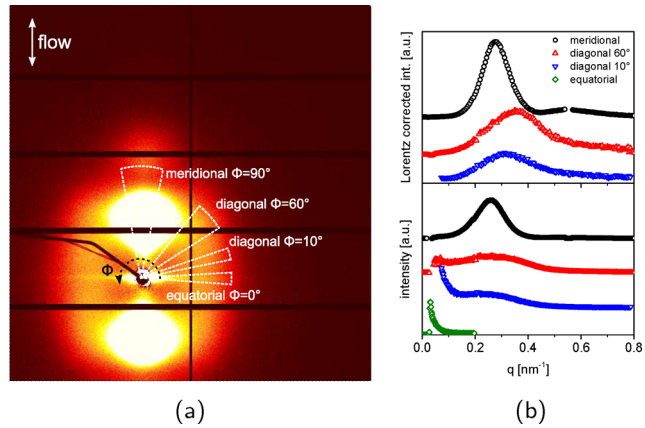

Figure 4. (a) 2D SAXS pattern collected at the end of the isothermal crystallization at 400 bar after being sheared for 0.25 s (v_{piston} = 80 mm/s). (b) Integrated intensities (bottom) and Lorentz corrected intensities (top) as a function of the scattering vector for the azimuthal regions shown in (a). The diagonal intensities were multiplied by a factor of 5, and the curves were shifted vertically for the purpose of clarity.

To obtain the time evolution of the equatorial and meridional intensities, related to the formation of shish and parents lamellae (kebabs), respectively, the 2D SAXS patterns were integrated azimuthally in the meridiodal (centered at ϕ = 90°) and equatorial region (ϕ = 0°) as shown in Figure 4a to obtain 1D scattering profile according to

$$I_{SAXS} = \int_0^{q_{max}} \int_{\phi_{min}}^{\phi_{max}} I(\phi, q)\, d\phi\, dq \quad (3)$$

where q_{max} is chosen to be 0.2 nm^{-1} for the equatorial region and 1.2 nm^{-1} for the meridional region; ϕ_{min} and ϕ_{max} are the minimum and maximum values of the azimuthal angle for the chosen region (ϕ_{min} = −5° and ϕ_{max} = 5° for the equatorial region and ϕ_{min} = 80° and ϕ_{max} = 100° for the meridional region). The peak shift of the SAXS maximum in the meridional region, related to the time evolution of the spacing between parents lamellae, were obtained from the position of the maxima, q^*, of the meridional integrated intensity according to Bragg's law: $L_p = 2\pi/q^*$.

3. RESULTS AND DISCUSSION

Because of the big amount of experimental data collected in this work, the results are presented and discussed in several subsections throughout this section: for each subsection the experimental observations are first discussed comparing different flow conditions (piston speeds) at the same initial pressure level and successively comparing different pressures at the same flow conditions. Only the experiments performed at the highest pressure (400 bar) at different piston speeds and the experiments with the highest piston speed (80 mm/s) at the four different pressures are selected as representative and shown in this section. A full overview of all the experimental results can be found in the Supporting Information.

We first focus on the rheological evolution during flow, i.e., the transient pressure drop, followed by the outcome of in situ X-ray analysis. For the SAXS data analysis the evolutions of the equatorial and meridional intensities are presented and discussed, together with the evolution of the spacing between α-parents lamellae. Later the apparent crystallinity and the apparent amount of α-, β-, and γ-phases obtained from WAXD

DOI: 10.1021/acs.macromol.7b00595
Macromolecules 2017, 50, 3868−3882

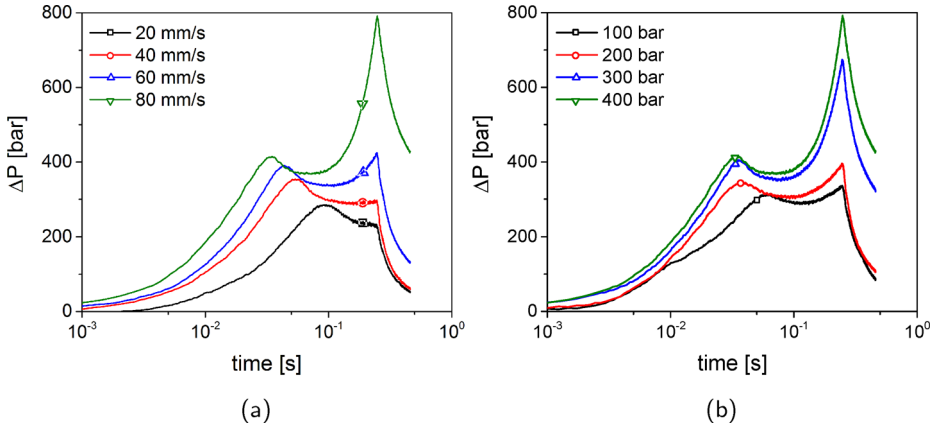

Figure 5. Transient pressure drop measured between the transducers during flow with four different piston speeds at 400 bar (a) and for different initial pressure levels using a piston speed of 80 mm/s (b).

analysis are examined. Finally, we focus solely on the evolution of the oriented iPP's lamellae in different morphologies: for this aim the ratios between α-parents/α-daughters, α-parents/γ-daughters, and α-daughters/γ-daughters are shown and compared.

3.1. Pressure Response. Figure 5a shows the measured pressure difference (ΔP) during and immediately after flow for the four different flow conditions employed at 400 bar. Clearly, the higher the flow rate (piston speed), the bigger the deviation from the typical viscoelastic behavior of a polymer melt subjected to start-up Poiseuille flow. This deviation is characterized by an upturn of the pressure drop after start-up, which was related in previous works[38,39] to structure formation (shish) in the high shear rate regions close to the walls. This structuring locally increases the viscosity of the material and therefore decreases the deformation rates close to the wall. Since the volumetric flow rate prescribed by the movement of the pistons stays the same, the shear rate experienced by the material just outside the shear layer increases, causing the formation of more shish and the thickening of the shear layer from the walls toward the center of the channel until flow is stopped. Rheologically, this translates to the observed upturn since the same amount of material is being pushed through a channel with decreasing cross section.

Increasing the velocity of the pistons causes a faster shish development, and consequently the formation of thicker shear layers (for the same flow times) and pronounced upturns in the pressure drop are observed. After stopping the flow, the pressure drop relaxes toward zero, meaning that the final pressures at the two transducers (and anywhere along the channel length) relax back to initial set values and the majority of the subsequent crystal growth happens in isobaric conditions.

Figure 5b shows the comparison of the pressure drop for different initial pressures at the same flow condition (piston speeds of 80 mm/s). The flow start-up (the time scale to reach steady state) is independent from the initial pressure for the same piston speed, since the dominant time scale is the compressibility as already stated in ref 39 and observed by Hatzikiriakos and Dealy.[40] The discrepancy for the start-up time, observed for the experiment performed at 100 bar, is an experimental artifact due to the top piston partially covering the top pressure transducer at the beginning of flow.

Similarly to the effect of flow, main differences are found in the behavior after start-up: the steady-state level of the pressure drop increases, and the observed deviation from viscoelastic behavior starts earlier and becomes more pronounced, increasing the initial pressure level at which flow is applied.

It is well know that the rheological properties[41,42] and therefore relaxation times change with pressure. Specifically, the pressure shift factor (a_p) can be defined by an exponential dependence from pressure (p):

$$a_p = \exp[k(p - p_{\mathrm{ref}})] \tag{4}$$

where for isotactic polypropylene k = 16.18 GPa^{-1} and p_{ref} = 1 bar.[42]

The characteristic rheological stretch relaxation time of the high molecular weight tail for the selected iPP, $\tau_{\mathrm{R}}^{\mathrm{HMW}}$, is equal to 0.23 s at 145 °C and 1 bar[29] (evaluated from the longest mode of a discrete Maxwell spectrum fitted on dynamic rheology measurements). When shifted to the experimental pressures of 100 and 400 bar, using eq 4, this increases from 0.27 to 0.43 s, respectively. This means that for the same flow conditions the high molecular weight tail of the material, responsible for the formation of shish, is more stretched when pressure is higher. Shish can form earlier in time, and the shear layer can develop faster, i.e. become thicker, and therefore, a stronger rise in the pressure drop is observed during flow at higher pressure.

3.2. "A Critical Note on the Criterion for Shish Formation". Our rheology results clearly show a straightforward dependence of the onset time for shish formation on the piston velocity, i.e., the wall shear rate ($\dot{\gamma}_{\mathrm{w}}$) and the initial pressure (acting on the rheological relaxation times). This is often combined in terms of the flow strength that is expressed by the Weissenberg number Wi:

$$\mathrm{Wi} = \tau_{\mathrm{R}}^{\mathrm{HMW}}(T, p)\dot{\gamma}_{\mathrm{w}} \tag{5}$$

Molecular stretch will occur when a critical value of the Weissenber number will be exceeded (Wi > Wi_{crit}).[43] The criterion for the formation of oriented structure from polymer melts has been subject of debate for already several decades and represents a topic of great relevance, since it is of paramount importance to predict whether or not the final product will be anisotropic, depending on the processing conditions employed. It is widely recognized that the stretch of the high molecular weight (HMW) tail of the material is key for the formation of oriented structures:[16,43−48] portions of long chains between topological constraints, i.e., entanglements, are more easily stretched because of their larger Rouse time.

DOI: 10.1021/acs.macromol.7b00595
Macromolecules 2017, 50, 3868−3882

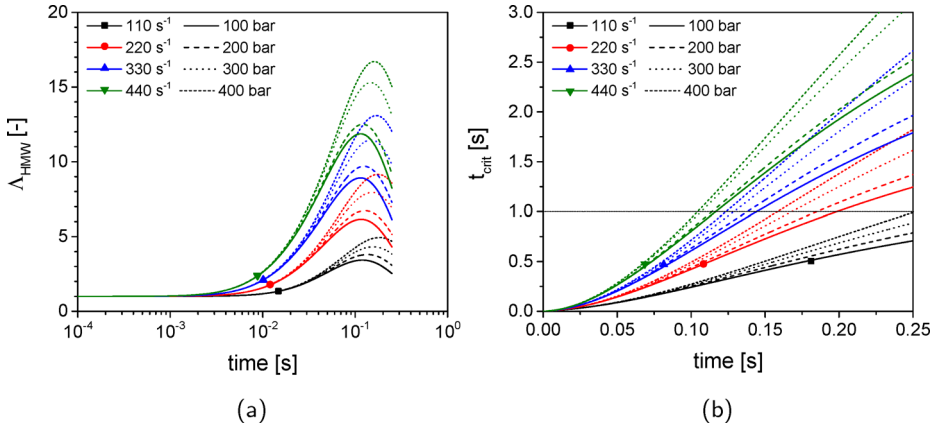

Figure 6. Molecular stretch of the high molecular weight tail (a) and time integral over the HMW molecular stretch history (b) computed in time (t_{shear} = 0.25 s) using a single-mode XPP for all the flow conditions and pressure employed. The horizontal line indicates the critical value of the cumulative stretch time.

It is also known that the combination of flow strength and duration of flow affects the formation of oriented crystals in a complicated way, and several hypotheses have been suggested. The simplest way to introduce the effect of flow duration (t_s) as the total applied strain ($\gamma = \dot{\gamma} t_s$) simply does not work: experimental evidence shows that strong shear flow for short time are much more effective than long flow at low shear rates.[29,47]

Focusing on the work performed in our group, several hypothesis were put forward. Basing their theory on rubber elasticity and molecular rheology, Van Meerveld et al. proposed that the transition to fibrillar structures takes place for certain critical value of the Weissenberg number related to chain stretch of the HMW fraction (Λ_{HMW}).[43] This is defined as $\Lambda_{HMW} = L_{HMW}/L_{0,HMW}$ where L_{HMW} and $L_{0,HMW}$ are the contour lengths of the HMW molecules during and before stretch, respectively, and the contour length is a smoothed path through the atomistic configuration of the backbone. The duration of flow was not directly taken into account, but the hypothesis of a critical value of the molecular stretch ratio to be exceeded takes the flow duration implicitly into account. In ref 49 a critical value for the HMW-stretch seemed to work quite well for a set of experiments similar to the ones performed in this work. However, the analyses were based on the assumption that during flow, the HMW-tail molecules deformed affinely, and this assumption was wrong (see HMW molecular stretch evolutions in Figure 6a). On the basis of experimental observations, van Erp et al.[23] proposed that not the momentary molecular stretch (Λ_{HMW}, evaluated fitting the nonlinear viscoelastic constitutive model (XPP)[50] to extensional rheology data) should be taken into account as such as a criterion for the initiation of shish growth, but its history over the shear time. A critical effective stretch time was introduced, defined as

$$t_{crit} = \int_0^{t_s} \Lambda_{HMW}(t)\, dt \tag{6}$$

which is the most simple way to account for the history of the HMW stretch. This approach proved valuable for predicting a series of results from dilatometry combined with shear flow experiments and was recently successfully applied by Van Drongelen et al.[51] for the FIC behavior of LLDPE in shear at different pressures.

Here we test this criterion on our experimental data using a simplified version of a complete model for flow-induced crystallization[39] and correlating the model results for shish formation with the onset times of the deviation from the regular viscoelastic behavior in the measured pressure drop. "Simplified" means that the flow is considered to be incompressible and isothermal (no shear heating), and only the wall shear (the highest shear rate) is considered. This makes this approach applicable for the determination if shish formation occurs without using a full numerical model based on finite element simulations.

Knowing the slit dimensions, the volumetric flow, and the power law behavior of the viscosity, the wall shear rates can be evaluated using[52]

$$\dot{\gamma}_{wall} = \frac{Q(1/n + 2)}{2w(h/2)^2} \tag{7}$$

where h and w are the slit thickness and width, $Q = h \times w \times v_{piston}$ the volumetric flow, and $n = 0.47$ the power law exponent obtained fitting the results of frequency sweep linear rheological measurements shifted to the experimental T and P. The evaluated wall shear rates for different piston speeds are presented in Table 1. These shear rates are the driving forces in the XPP model.[50]

Table 1. Wall Shear Rates for Stationary Flow, Calculated from Eq 7 for the Four Different Piston Speeds

piston speed [mm/s]	20	40	60	80
$\dot{\gamma}_{wall}$ [s^{-1}]	110	220	330	440

The HMW-stretch Λ_{HMW} is obtained from a simplified form (the Giesekus parameter $\alpha = 0$) of a single-mode XPP model given by

$$\overset{\nabla}{\mathbf{c}} + 2\frac{\exp[\nu_i(\sqrt{\mathrm{tr}\,\mathbf{c}/3} - 1)]}{\tau_R^{HMW}}\left(1 - \frac{3}{\mathrm{tr}\,\mathbf{c}}\right)\mathbf{c} + \frac{1}{\tau_0}\left(\frac{3\mathbf{c}}{\mathrm{tr}\,\mathbf{c}} - \mathbf{I}\right) = 0$$
$$\Lambda_{HMW} = \sqrt{tr(\mathbf{c}/3)} \tag{8}$$

in which $\overset{\nabla}{\mathbf{c}}$ and tr $\mathbf{c}$ are the upper convected derivative and the trace of the conformation tensor ($\mathbf{c}$), respectively, $\tau_0(T,p)$ is the orientation relaxation time, and ν is the reciprocal of the number of arms. The parameter values for evaluating t_{crit} are available from ref 39. Although these showed good results in the case of van Erp et al.,[24] we noticed that the stretch relaxation times, obtained from fitting the XPP model to

DOI: 10.1021/acs.macromol.7b00595
Macromolecules 2017, 50, 3868−3882

extensional data, are much too long for the flow times used in this work, showing no difference during flow for the cumulative molecular stretch at different pressures. Better and more physical results are found if the Rouse time for the HMW tail extracted from linear rheology measurements[29] is used, i.e.

$$\tau_R^{HMW}(T, p) = \frac{\tau_0(T, p)}{3Z} \tag{9}$$

where τ_0 is obtained from the longest mode of the linear viscoelastic spectrum and $Z = M_w/M_e = 70$, using a value of $M_e = 5200$ g mol^{-1}.[53] The results are shown in Figure 6a (HMW-stretch, Λ_{HMW}) and b (critical stretch time, t_{crit}).

A critical value of the cumulative stretch time of 1 s is consistent with the onset time of shish formation evaluated from the pressure rise observed in experimental results given in the Supporting Information (Figures S1 and S2); see Figure 7.

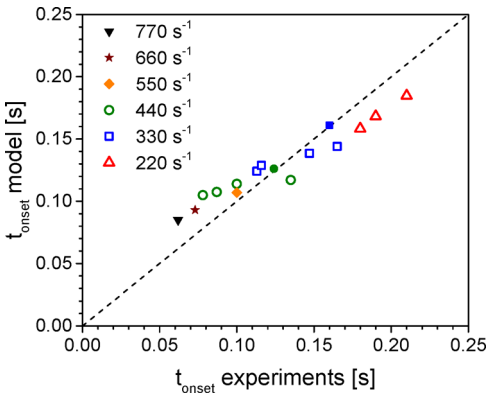

Figure 7. Comparison between the shish onset times predicted for a critical stretch time of 1 s and the shish onset time measured from the upturn in the pressure drop for different wall shear rates. Full markers represent the predictions for the experiments taken from ref 49.

Good agreement is found; at high shear rates (440−330 s^{-1}) the model slightly overpredicts the experimental results whereas for lower shear rates the opposite is observed. Experimentally, no shish formation (i.e., no pressure upswing) is found for a piston speed of 40 mm/s (wall shear rate 220 s^{-1}) at a pressure of 100 bar and for a piston speed of 20 mm/s (wall shear rate 110 s^{-1}) at all pressures. The model predicts shish formation for the first condition only. Moreover, the same approach works for the same set of experiments perfomed at lower pressure (50 bar) in ref 49 (see full markers in Figure 7). Although a relatively simple model is used, i.e., isothermal (no shear heating taken into account) and incompressible flow, the results give strong support to the hypothesis that formation of oriented structures is not related to a value of the molecular stretch of the HMW tail but to the "stretch history" during flow time.

This is summarized in the following important observations:

- Using a one-mode simplified XPP model, we can capture the important part of the rheology of the material that dominates flow-induced crystallization, i.e., the contribution of the HMW-tail, which hardly contributes to the total shear stress and thus to the mechanical work applied.
- It is the history of the HMW-stretch that controls the onset of shish formation. The most simple way to account for the history (see eq 6) gives already very satisfactory results (see Figure 7). Model and experimental results differ only in the order of 10%, and also the absence of shish formation during flow is captured quite well.
- It is of utmost importance to take into account the temperature and pressure dependency of the stretch relaxation time.
- This stretch relaxation time should be based on molecular considerations, i.e., the MW of the tail, and not on fitting rheological data.
- The average initial pressure was used. Taking into account the influence of the increased pressure due to the flow on the relaxation times did not make a real difference.

Considering recent work from our group, it should be noticed that there are some clear differences in the approach used. First of all, in van Erp et al. the value for the critical stretch time used was $t_{crit} = 45$ s.[24] This value is based on the high Rouse time used in that work and obtained by comparing critical stretch time values at the end of the flow. These values were then used to discriminate between experiments in terms of the presence/absence of shish; it was not used for predicting the onset of shish formation that could not be observed in the type of experiments they performed.

Second, Roozemond et al. performed numerical simulations on a slit flow similar to the one described in this paper.[39] They

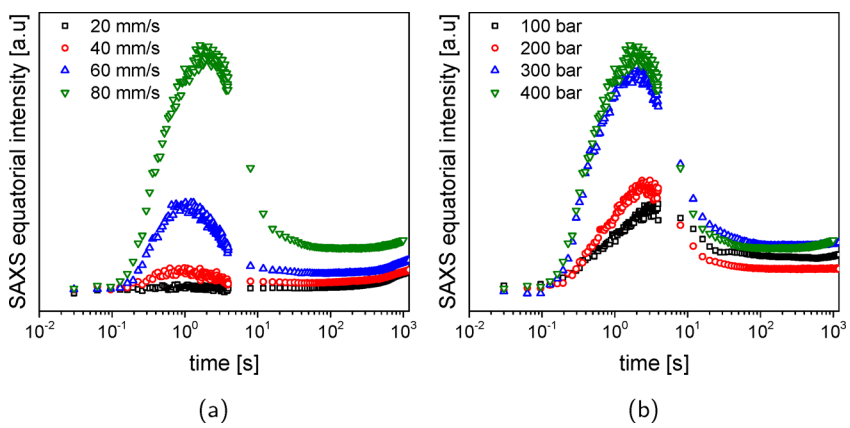

Figure 8. Equatorial SAXS integrated intensity evolutions during the first 20 min for all flow conditions and a pressure of 400 bar (a) and for different initial pressures and a piston speed of 80 mm/s (b).

DOI: 10.1021/acs.macromol.7b00595
Macromolecules 2017, 50, 3868−3882

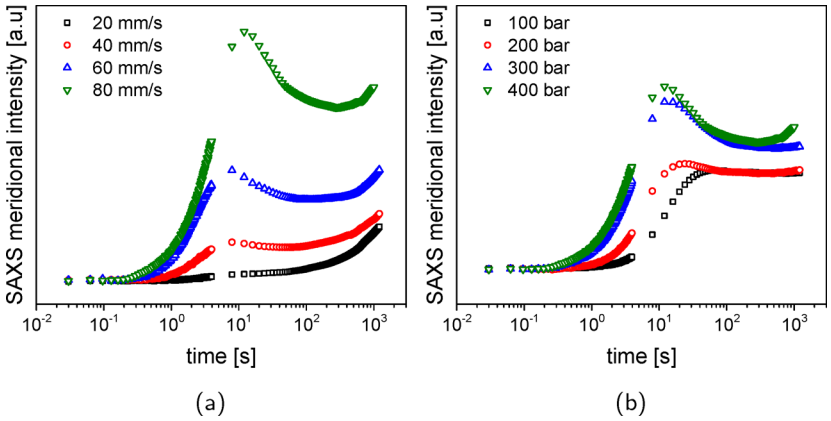

Figure 9. Meridional SAXS integrated intensity evolutions during the first 20 min for all flow conditions and a pressure of 400 bar (a) and for different initial pressures and a piston speed of 80 mm/s (b).

did not use any criterion for shish formation at all. In their approach flow-enhanced nucleation has pressure and temperature dependence, but the rate of shish formation is proportional to the shear rate only; i.e., there is no temperature or pressure dependency in the latter. As no controlled pressure variation was applied, there was no need to consider this aspect. However, for such a complete and complex model, which takes into account all effects (compressibility, nonisothermal) and the coupling between structure formation and rheology, it is hard to judge which part(s) of the model are most determining for the phenomena we are looking at. Further work on this full finite element model is required to find out which approach is the most promising and this ongoing work. However, the simplicity of the model, as presented here, makes it a very useful approach for determining if, for a given material and thermal and flow conditions, one can expect shish formation during flow or not.

3.3. SAXS Analysis. *3.3.1. SAXS Equatorial Intensity Evolutions.* The time evolutions of the SAXS equatorial intensity (related to shish structures, see section 2.2.4) are presented in Figure 8 comparing the four different flow conditions at a pressure of 400 bar (a) and the four different pressures using the fastest piston speed of 80 mm/s (b).

At 400 bar (Figure 8a), the SAXS equatorial intensity, related to the formation of bundles of chains aligned in flow direction (shish), starts to increase already during flow for piston speeds ranging from 40 to 80 mm/s, whereas for 20 mm/s no detectable increase is found, in agreement with the rheological behavior observed in Figure 5a. The increase of the SAXS equatorial intensity has a delay compared to the upturn in the pressure drop for all pressures and flow conditions. As hypothesized by Ma et al.[49] for similar experiments conducted at ambient pressure and confirmed by numerical finite element simulation on the same flow geometry,[39] the shear layer formation starts upstream (close to the driving piston), and this is reflected into the pressure upturn. The shish formation happens later in the middle of the slit (at the diamond window), where X-ray measurements are done. As expected, the highest value reached by the equatorial intensity is higher for faster flow rates because thicker shear layer are formed increasing the velocity of the piston. The increase lasts for about 1−3 s, depending on the flow condition and pressure, although the formation and longitudinal growth of threadlike precursors take place mostly when the deformation is applied, i.e., during flow. The observed increase after flow is explained by the "densification" of shish when the flow has ceased, which according to recent findings[17] can been related to unidirectional propagation of a growth front along the shish backbone.

After the first increase, the equatorial intensity decreases significantly: this can be related either to dissolution of part of the shish structures formed by flow[54] or, more likely, to a decrease of electron density fluctuations in the direction perpendicular to flow, due to the growth of parent lamellae (kebabs) nucleating from the shish backbone which increase the electron density in the regions between shish. This will be clarified in the next subsection. When comparing the fastest piston speeds experiments at different pressures (Figure 8b), the increase of the SAXS equatorial intensity is clear in all cases, and similarly to the effect of flow, differences can be found in the onset time of the increase of the equatorial intensity and on its maximum value.

The already discussed increase of relaxation times with pressure causes an enhanced formation of shish and, therefore, a sooner onset in the increase of the SAXS equatorial intensity. Moreover, the formation of thicker shear layers at higher pressure translates in higher maximum values of the equatorial intensity for higher pressure.

3.3.2. SAXS Meridional Intensity and Spacing between α-Parents Evolutions. As well as the shish formation, also the growth of kebabs (parents lamellae) nucleating from the shish backbones is influenced by both flow rate and pressure. This is evident from the time evolutions of the SAXS meridional intensity plotted in Figure 9 for different piston speed at 400 bar (a) and at different pressure for the fastest piston speed (b).

If we consider the experiments performed at 400 bar (Figure 9a), the SAXS meridional intensity starts to increase immediately after flow stops, indicating the development of kebabs growing perpendicularly to flow direction (α-parents). Increasing the velocity of the piston causes a sooner onset of their growth because of a dual effect of flow: at higher shear rates more shish are formed, providing more nucleation sites for parents lamellae, and higher residual orientation is present close to the shish backbones, promoting a faster growth of the parent lamellae morphology. This last point will be explained in more detail in sections 3.4.1 and 3.4.3. Note that in all cases the meridional intensity reaches significant values after about 1−3 s (about 20% of its highest value), corresponding to the observed decrease in equatorial intensity. This confirms our previous hypothesis that the decrease in the scattering due to the shish can be explained by the decrease in electron density

DOI: 10.1021/acs.macromol.7b00595
Macromolecules 2017, 50, 3868−3882

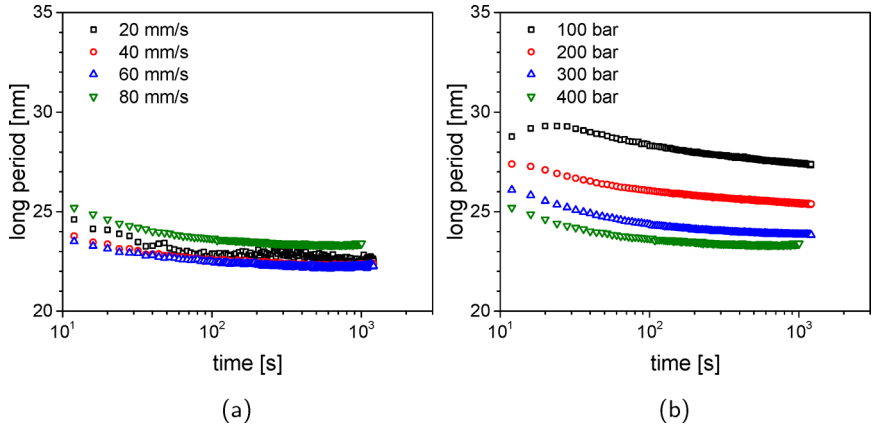

Figure 10. Time evolutions of the long period between α-parent kebabs during the first 20 min for all flow conditions and a pressure of 400 bar (a) and for different initial pressures and a piston speed of 80 mm/s (b).

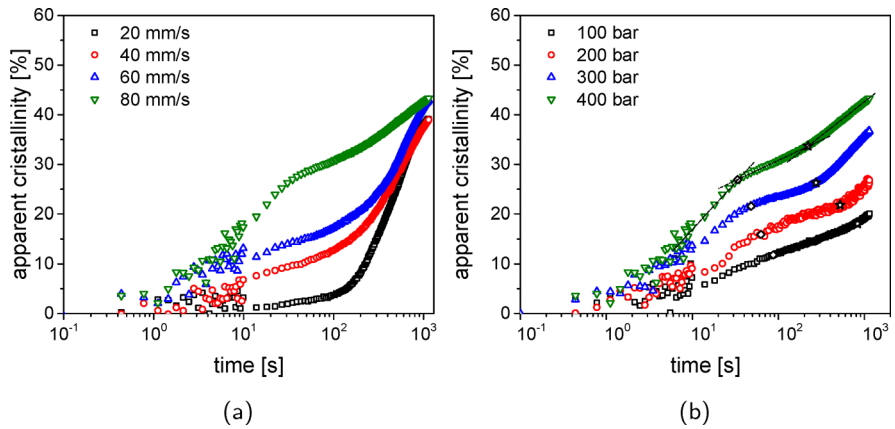

Figure 11. Time evolutions of the apparent crystallinity for all flow conditions and a pressure of 400 bar (a) and for different initial pressures and a piston speed of 80 mm/s (b). Open stars and diamonds markers (☆ and ◇) represent the onset of the formation of the fine-grained and isotropic layer, respectively.

fluctuations between shish caused by kebab overgrowth. The small decrease of the SAXS meridional intensity observed after about 10 s from the beginning of flow can be explained in a similar way: the branching of daughter lamellae (α- and γ-daughters) from the kebabs decreases the electron density fluctuactions in the direction parallel to flow (between kebabs), causing a decrease in the intensity scattered in the meridional region of the reciprocal space. The final increase of the SAXS meridional intensity (after about 200−500 s depending on the flow conditions) can instead be related to the contribution to the scattering of isotropic lamellae, constituting spherulites in the core of the sample.

The influence of pressure on the SAXS meridional intensity for the experiment performed with a piston speed of 80 mm/s is presented in Figure 9b. Also in this case the effect is evident: higher pressure induces a faster growth of parent lamellae as becomes clear from the sooner onset in the rise of the SAXS meridional intensity. This can be explained in the light of the pressure dependence of the crystal growth rate: α-phase kebab growth rate is increased of about a factor 6.3 at 145 °C for an increase of pressure from 100 to 400 bar.[30] Moreover, an increase of pressure also boosts the number of nucleation sites for the kebabs on the shish backbones by decreasing the nucleation free energy barrier and promoting the nucleation of parent lamellae on shish lateral surfaces.

This is clear from the time evolutions of long period of the α-parent kebabs presented in Figure 10. If the effect of the flow rate on the spacing between α-parents (Figure 10a) is not relevant, since solely dictated by the temperature and pressure at which the experiment is performed (in all the experiments performed at 400 bar, the average long period decreases from 25 to 23 nm during the 20 min of isothermal crystallization), the effect of pressure shown in Figure 10b is evident. The experiment performed at the highest pressure (400 bar) shows a final long period of about 23 nm whereas the one performed at 100 bar of about 28 nm: higher pressure results in a smaller long period between α-parent kebabs. The shish lateral surfaces can nucleate more lamellae at elevated pressure, when the nucleation free energy barrier is lower and the resulting spacing is denser.

3.4. WAXD Analysis. *3.4.1. Apparent Crystallinity and Phase Content Evolutions.* Figure 11 shows the time evolutions of the apparent crystallinity at 400 bar for the four different piston speeds (a) and at different pressures for the experiments performed with a piston speed of 80 mm/s (b).

For all flow conditions at 400 bar (Figure 11a), we observe the characteristic S-shaped curve indicative of crystallization until impingement, which occurs around 20 s after the beginning of flow. Therefore, we conclude that for this pressure this time scale includes the crystallization of highly oriented crystalline structures close to the walls (shear layer). After

DOI: 10.1021/acs.macromol.7b00595
Macromolecules 2017, 50, 3868−3882

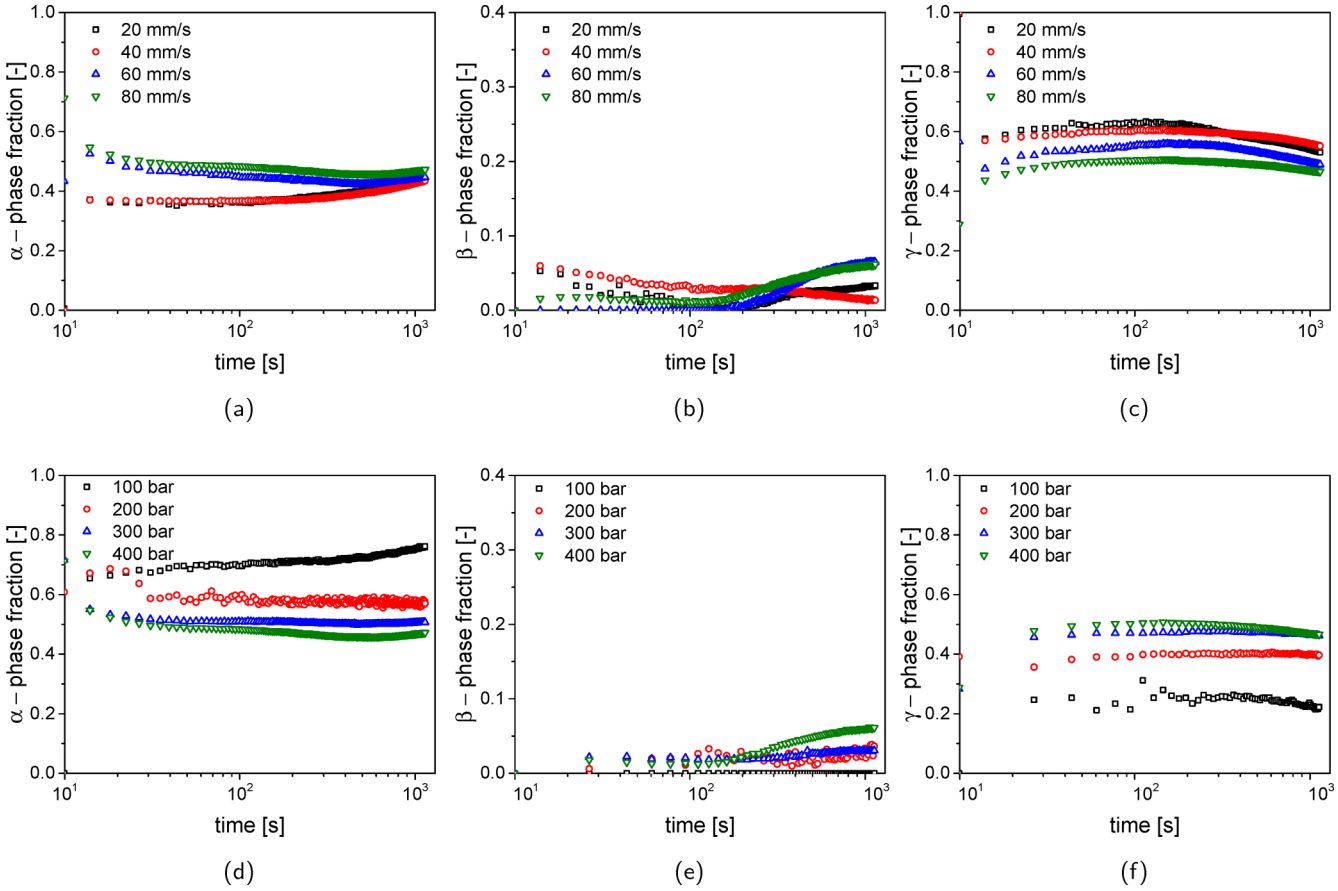

Figure 12. Time evolutions of the α- (a, d), β- (b, e), and γ-phase (c, f) fractions for all flow conditions and a pressure of 400 bar (a–c) and for different initial pressures and a piston speed of 80 mm/s (d–f).

impingement of the shish-kebab structures, the apparent crystallinity continues to increase with a lower slope until about 100 s. This can be ascribed to the development of less oriented crystals growing from less densely packed oriented nuclei in the fine-grained layer, defined as sausages by the Kornfield group.[55]

After the first 100 s, the apparent crystallinity undergoes a further increase, which is bigger for the slower flow rates experiments (for 20 mm/s the increase is of about 30% whereas for 80 mm/s is about 10%), until reaching a final level comprised between 38% and 43%. This observation is ascribed to the crystallization of isotropic structures (spherulites) in the middle of the channel.

The experiments performed with the fastest piston speed at different pressure levels (Figure 11b) are illustrative of the effect of pressure on the crystallinity development during and after flow. For all pressures, the crystallinity first increases sharply, then with a lower slope, and finally a last increase is observed. This is again related to the development of the shear layer, fine grain layer, and the isotropic core, respectively, resulting from the different shear rates experienced by the material along the slit thickness. As expected, differences are found in the onset of crystallinity development for the different layers, which clearly develop faster at higher pressure. As already discussed in sections 3.1 and 3.3.1, the shear layer is formed sooner at higher pressure due to the dependence of the relaxation times on pressure. Moreover, within the shear layer, parents and daughters lamellae nucleating from shish and kebabs, respectively, grow faster when the pressure is higher due to the pressure dependency of the growth rates of both α- and γ-phases.[30] Consequently, the shear and the fine grained layers can be filled in shorter times, increasing the pressure. Finally, the different levels of apparent crystallinity observed for different pressures (higher at higher pressure) are readily explained by the different thickness of the shear layers and by an increased nucleation density and crystal growth rate in the isotropic core. Evaluating the quiescent crystallization kinetics at 145 °C and at the different pressures employed in this work, using the crystallization model developed in our group by Van Drongelen et al.,[30] we find the onset of crystallization to be at 1200, 476, 326, and 167 s for pressures of 100, 200, 300, and 400 bar, respectively. The onsets of the last crystallization process (890, 522, 273, and 220 s, evaluated from the intersections of the slopes indicated with the dotted lines in Figure 11b), that we related to the crystallization of the isotropic layer, are faster than the predicted ones. This can be easily explained since, as already pointed out before in this work, the apparent crystallinity represents an average of the crystal fraction over the entire thickness of the flow cell, which experiences different shear rates. Therefore, the isotropic layer itself is composed of regions with a gradient of nucleation densities (which decrease moving from the fine grained layer to the middle of the slit), whereas the crystallization model prescribes a fixed nucleation density for isothermal and isobaric conditions.

Figure 12 shows the time evolution of the fractions of different phases, α (a, d), β (b, e), and γ (c, f) evaluated according to eq 2, during the isothermal crystallization at a

DOI: 10.1021/acs.macromol.7b00595
Macromolecules 2017, 50, 3868–3882

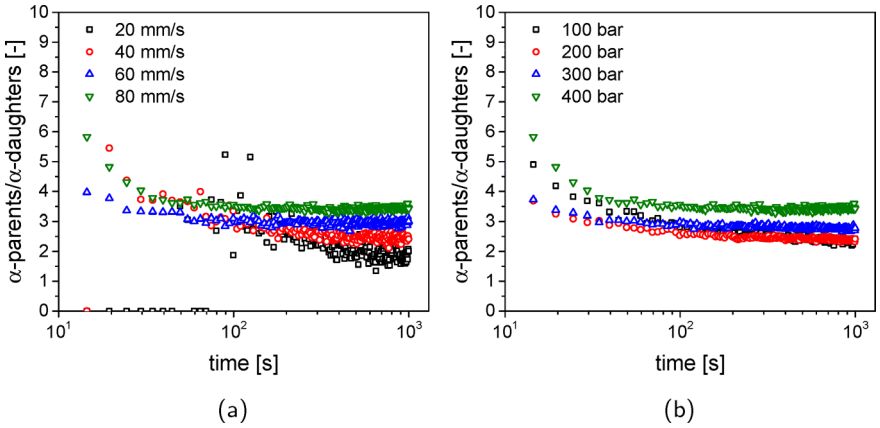

Figure 13. Time evolutions of the α-parents/daughters ratio for all flow conditions and a pressure of 400 bar (a) and for different initial pressures and a piston speed of 80 mm/s (b).

pressure of 400 bar after flow with different piston speeds (a–c) and at different pressure levels after flow applied using a piston speed of 80 mm/s (d–f).

For the experiments performed at 400 bar using different piston speeds (Figure 12a–c), two main observation can be extracted: α- and γ-phases are the predominant polymorphs, with the α-phase promoted by faster flow rates, and a small amount of β-phase develops after flow (about 5%) for all flow conditions independently of piston speed used.

The observed dependence of the amount of γ-phase from the flow rates is the result of the complex morphology evolution found in flow-induced crystallization of iPP at elevated pressures consisting of α-parents kebabs, growing from the shish lateral surfaces, from which α- and γ-daughters lamellae can nucleate and grow (see Figure 4c). After shish structures, which consist of α-phase, are formed during flow, some residual orientation of the polymer chains is still present close to the shish backbones. This residual orientation is higher for faster flow rates and promotes the growth of α-parents lamellae since the chains are oriented in the *c*-axes directions of their unit cells (parallel to flow): the result is that α-phase formation is boosted at higher flow rates due to a faster growth of the parents lamellae.

The rather constant and low amount of β-phase observed can be explained in light of a limited region of space where it can be nucleated and lower crystal growth rate compared to the other two polymorphs. It is well-known that β-phase can be nucleated either by specific nucleating agents[56−58] or by shear-induced α-row nuclei.[12,59] Clearly, in these observations, the presence of β-crystals is ascribable to the latter case: as reported by Housmans et al.[6] in injection-molded iPP and by Ma et al. during experiments performed using the same setup employed in this work,[10] β-phase is mostly present in the fine-grained layer. This means that β-crystals are confined in a very narrow region of channel cross section, contributing little to the overall crystallinity observed, which is an average over the entire channel thickness. Moreover, they are growing in competition with α- and γ-phase crystals, which have a much higher growth rate for the experimental conditions employed in this work (145 °C and 400 bar).[30] Therefore, only a little amount of β-phase can grow in the fine-grained layer, before the space is filled by the other two polymorphs.

Focusing on the effect of pressure (Figure 12b), it is clear that, as expected, γ-phase formation is promoted by pressure at the expenses of the α-phase: increasing the pressure from 100 to 400 bar results in more than doubling the amount of γ-phase. This is easily explained by the enhancement of γ-phase growth observed upon pressurization: using experimental crystallization data on the same iPP grade,[30] it is found that the growth rate of the γ crystals is similar to the one of α-phase at 145 °C and 400 bar ($G_\gamma/G_\alpha \simeq 0.8$) and decreases to about $G_\gamma/G_\alpha \simeq 0.5$ at 100 bar, in rather good agreement with the ≃50% and ≃25% of γ-phase found at 400 and 100 bar, respectively. Finally, similarly to flow, no clear effect of pressure can be found on the formation of β-phase crystals.

3.4.2. α-Parents/α-Daughters Ratio Kinetics. Further insight into the complex morphological development of shish-kebabs with α- and γ-phase lamellar branching can be obtained by the analysis of the ratios of parent and daughter species. We point out again that these ratios are obtained from the azimuthal distributions of the $(130)_\alpha$ and $(117)_\gamma$ reflections after subtraction of the amorphous scattering and the contribution to diffraction of isotropic crystals. The ratios are therefore only indicative of the amounts of α- and γ-phase lamellae developing in the shear and in the oriented part of the fine-grained layer, where solely oriented crystals are present.

Figure 13 shows the effect of flow rates (a) and pressure (b) on the time evolution of the ratio between α-parents and α-daughters lamellae. For all flow conditions at 400 bar (Figure 13a), this ratio is initially higher after flow and subsequently decreases during the first 100 s of isothermal crystallization, reaching a constant value when the shear layer and fine-grained layers reach full space filling. The observation is easily explained by the initial growth of parent lamellae from the shish backbones and from the subsequent growth of α-daughters nucleating from the parents.

The α-parents/α-daughters ratio is higher at higher flow rates (piston speeds) because of the already discussed increased α-parents growth rate after flow: higher residual orientation close to the nucleating shish lateral surfaces at faster piston speeds promotes the growth of α-parents since their *c*-axes are oriented in flow direction, whereas the flow-induced conformation makes crystallization in the daughter morphology less favorable. If big part of the space in the shear layer is filled by the parents during the time immediately after flow, daughters will have less volume available to grow. An increased amount of α-parents at faster imposed flow rates was already observed by Kumaraswamy et al.[60] during experiments performed using a slit-flow shear cell coupled with SAXS/WAXD. Their speculation was that the experimental observation was related to an enhanced

DOI: 10.1021/acs.macromol.7b00595
Macromolecules 2017, 50, 3868−3882

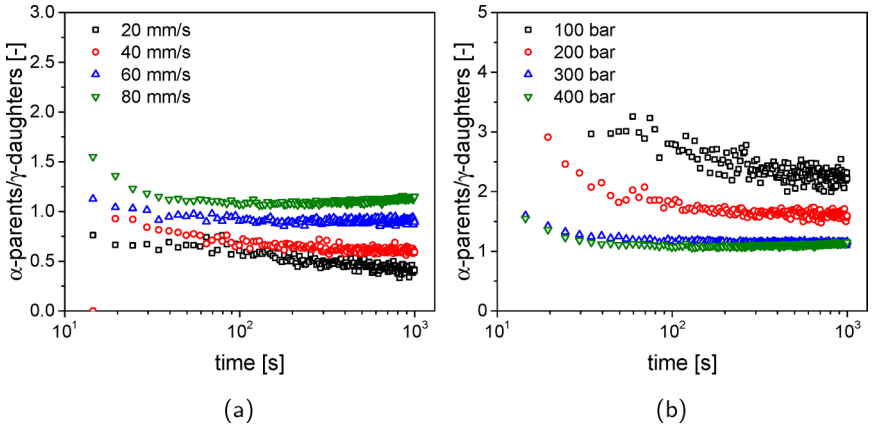

Figure 14. Time evolutions of the α-parents/γ-daughters ratio for all flow conditions and a pressure of 400 bar (a) and for different initial pressures and a piston speed of 80 mm/s (b).

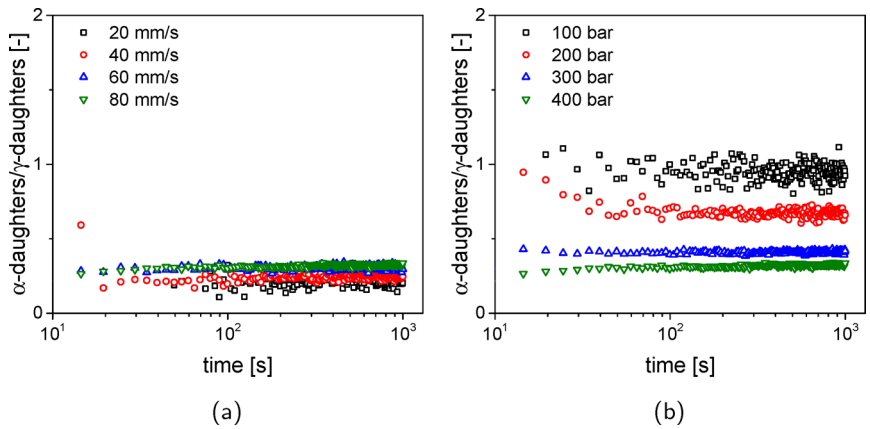

Figure 15. Time evolutions of the α-daughters/γ-daughters ratio for all flow conditions and a pressure of 400 bar (a) and for different initial pressures and a piston speed of 80 mm/s (b).

nucleation and growth of parents lamellae only during flow, since these have their *c*-axes aligned in the deformation direction. They also stated that after the cessation of flow, since stresses relax rapidly, the enhancement of parents lamellae formation would cease and the parents/daughters ratio would just be dictated by the crystallization temperature. Although reasonable, their statement was based on experiments with much longer flow times if compared to ours (up to 12 s), and due to the limitations of X-ray detectors at that time, the first experimental WAXD pattern was collected not during but immediately after flow. Since flow lasts only 0.25 s for our experiments, and no significant parents' growth is detected, the higher amount of α-parent lamellae can only be ascribed to an increased growth rate after flow stops.

A similar effect is found for level of pressure for flow applied with a piston speed of 80 mm/s (Figure 13b): the α-parents/α-daughters ratio is higher, i.e., more parents are formed, increasing pressure at which the experiment is performed. The effect of pressure in this regards is dual: the development of α-parents is boosted by both the increased the relaxation times (more orientation close to the shish backbones) and by a higher nucleation density on the shish backbones since the free energy barrier for nucleation is decreased by an increased pressure (see Figure 10b). Moreover, as proposed by Roozemond et al.[28,61] on the basis of experimental observation, the increased growth rate for the α-parents during and immediately after flow relaxes back to the quiescent value due to chains relaxing toward their equilibrium conformation, with a characteristic time scale corresponding to the average relaxation time. Therefore, not only α-parents can grow faster because chains are stretched more (flow is more effective) at higher pressure but also the duration of their increased growth is longer, since the residual orientation will last longer in time at higher pressure.

3.4.3. α-Parents/γ-Daughters Ratio Kinetics. The trends for the time evolutions of the α-parents/γ-daughters ratio are presented in Figure 14. As clear from Figure 14a, where the experiments at 400 bar with different piston speeds are shown, faster flow rates promote the formation of α-parents at the expenses of γ-daughters for the same reason discussed in the previous paragraph (increased growth rate of parents for higher molecular orientation). The effect is quite significant if we consider that the final amount of parents is about 2.5 times higher than the one of γ-daughters when decreasing the piston speed from 80 to 20 mm/s, similarly to what observed in Figure 13a for the α-parents/α-daughters ratio at these two flow conditions (in this case the amount of parents is higher of a factor 2). This confirms that when the flow rates are high, the molecular orientation enhanced growth rate of the parents will causes their overgrowth within the shear layer, reducing the free volume available for the daughters (in both α- and γ-phase).

The time evolution of the α-parents/γ-daughters ratio for the experiments performed using a piston speed of 80 mm/s and different pressures is shown in Figure 14b. As expected, a clear

DOI: 10.1021/acs.macromol.7b00595
Macromolecules 2017, 50, 3868−3882

dependence from the pressure is found: the α-parents/γ-daughters ratio decreases, increasing the pressure at which flow is applied.

3.4.4. α-Daughters/γ-Daughters Ratio Kinetics. Additional information on the multiphase, multimorphological development in the shear layer can be extracted from the evolutions of the ratios of α- and γ-daughters, presented in Figure 15, which grow in competition from the template of parent lamellae.

For the experiments performed at 400 bar and different flow conditions (Figure 15) the ratio between the two daughters morphologies is constant for the entire duration of the isothermal experiments and, surprisingly, much lower than 1 (γ-daughters are more abundant than α-daughter, although their relative growth rates are similar). This observation seems to be in line with the previous observation of van Erp et al.,[9] who observed a remarkably high amount of γ-daughters for sample crystallized at high pressure after shear. Their interpretation, lately supported by the modeling work of Roozemond,[28] was that γ-phase lamellae can nucleate also from the shish backbones, leading to higher amount than the one predicted by the relative growth rates. Moreover, no significant effect of the flow rate used is observed: clearly, residual orientation after flow has no influence on the formation/nucleation mechanisms of daughters developing in the two phases.

Finally, the influence of pressure can be appreciated from the analysis of Figure 15b: as expected, γ-daughters morphology is promoted by high pressure.

4. CONCLUDING REMARKS AND OUTLOOK

The results discussed in the previous sections showed that the complex polymorphism arising from flow induced crystallization of iPP at elevated pressure can be fully understood and therefore likely predicted from modeling on the basis of several basic concepts:

- Flow influences especially nucleation density, acting via molecular stretch. Shish are formed early in time, and the shear layer in the slit develops faster (and become thicker) when the volumetric flow rates are higher. Moreover, enhanced point nucleation is observed in the region of the channel which experiences lower shear rates: overall crystallization kinetics speed up tremendously.
- Our observations give support to the concept of a criterion for shish formation based on the history on the stretch of the high molecular weight fraction of the material.
- Flow influences the crystal growth rate of α-parents lamellae nucleating from the shish backbones, since molecular orientation is favorable to the formation of crystals with their chain axes parallel to flow. Consequently, more α-phase is found at higher flow rates.
- Pressure has a dual effect on nucleation: both the amount of oriented nuclei (shish) and the nucleation sites on them are affected. The increase of relaxation times (due to increase in pressure) enhances the effect of flow in creating shish structures: the more shish, therefore thicker shear layers, are formed at higher pressure. Moreover, the nucleation sites on shish for parents lamellae are increased by pressure because of the decrease in nucleation free energy. The isotropic layer experiences an increased nucleation density for the well-known increase in undercooling due to pressure.
- Quiescent growth rates of both α- and γ-phases are increased by pressure, with γ-phase being promoted by higher pressures. Growth rate of α-parents is also increased by pressure, since the relaxation times are increased and stronger molecular orientation is found close to the shish.
- A remarkably high amount of γ-daughters form at the expenses of the α-daughters for relatively high pressure, which cannot be explained only by the different growth rates of the two phases. The idea of γ-lamellae nucleating from the shish backbone could explain this observation.

This experimental work provides a rather complete and critical overview on the real-time structural evolution of iPP at elevated pressure, comprising different crystal structures and morphologies, which is fundamental for the understanding final properties of products industrially produced using the injection-molding technique. Promisingly, all the experimental observation are coherent with our previously developed crystallization modeling framework, and future work will focus on implementing it for elevated pressure conditions.

■ ASSOCIATED CONTENT

Supporting Information

The Supporting Information is available free of charge on the ACS Publications website at DOI: 10.1021/acs.macromol.7b00595.

Figures S1−S22 (PDF)

■ AUTHOR INFORMATION

Corresponding Author

*E-mail g.w.m.peters@tue.nl; Tel +31402474840 (G.W.M.P.).

ORCID

G. W. M. Peters: 0000-0001-7208-5128

Notes

The authors declare no competing financial interest.

■ ACKNOWLEDGMENTS

This research forms part of the research programme of the Dutch Polymer Institute (DPI), project #787. NWO (Nederlandse Organisatie voor Wetenschappelijk Onderzoek) is acknowledged for providing beamtime at the ESRF. The authors are grateful to the DUBBLE (Dutch Belgian beamline) staff at the ESRF for supporting the X-ray experiments. E.M.T. is grateful to Prof. Finizia Auriemma from University of Naples "Federico II" for the discussion and suggestions on X-ray data analysis and to Peter Roozemond (DSM Ahead) for the fruitful discussion and the remarks on the manuscript. Coen Clarijs (TU Eindhoven) and Rocco di Girolamo (University of Naples "Federico II") are gratefully acknowledged for the support during the experiments.

■ REFERENCES

(1) Schrauwen, B. A. G.; Breemen, L. C. A. V.; Spoelstra, A. B.; Govaert, L. E.; Peters, G. W. M.; Meijer, H. E. H. Structure, Deformation, and Failure of Flow-Oriented Semicrystalline Polymers. *Macromolecules* **2004**, *37* (23), 8618−8633.

(2) Mencik, Z.; Fitchmun, D. R. Texture of injection-molded polypropylene. *J. Polym. Sci., Polym. Phys. Ed.* **1973**, *11* (5), 973−989.

(3) Pantani, R.; Coccorullo, I.; Speranza, V.; Titomanlio, G. Modeling of morphology evolution in the injection molding process

DOI: 10.1021/acs.macromol.7b00595
Macromolecules 2017, 50, 3868−3882

of thermoplastic polymers. *Prog. Polym. Sci.* **2005**, *30* (12), 1185−1222.
(4) Kantz, M. R.; Newman, H. D.; Stigale, F. H. The skin-core morphology and structure-property relationships in injection-molded polypropylene. *J. Appl. Polym. Sci.* **1972**, *16* (5), 1249−1260.
(5) Fujiyama, M.; Wakino, T.; Kawasaki, Y. Structure of skin layer in injection-molded polypropylene. *J. Appl. Polym. Sci.* **1988**, *35* (1), 29−49.
(6) Housmans, J. W.; Gahleitner, M.; Peters, G. W. M.; Meijer, H. E. H. Structure-property relations in molded, nucleated isotactic polypropylene. *Polymer* **2009**, *50* (10), 2304−2319.
(7) Kalay, G.; Zhong, Z.; Allan, P.; Bevis, M. J. The occurrence of the γ-phase in injection moulded polypropylene in relation to the processing conditions. *Polymer* **1996**, *37* (11), 2077−2085.
(8) Kalay, G.; Bevis, M. J. Processing and physical property relationships in injection-molded isotactic polypropylene. 2. morphology and crystallinity. *J. Polym. Sci., Part B: Polym. Phys.* **1997**, *35* (2), 265−291.
(9) van Erp, T. B.; Balzano, L.; Peters, G. W. M. Oriented Gamma Phase in Isotactic Polypropylene Homopolymer. *ACS Macro Lett.* **2012**, *1* (5), 618−622.
(10) Ma, Z.; Balzano, L.; Portale, G.; Peters, G. W. M. Flow induced crystallization in isotactic polypropylene during and after flow. *Polymer* **2014**, *55* (23), 6140−6151.
(11) Baert, J.; van Puyvelde, P.; Langouche, F. Flow-Induced Crystallization of PB-1: From the Low Shear Rate Region up to Processing Rates. *Macromolecules* **2006**, *39* (26), 9215−9222.
(12) Somani, R. H.; Hsiao, B. S.; Nogales, A.; Fruitwala, H.; Srinivas, S.; Tsou, A. H. Structure development during shear flow induced crystallization of i-pp: In situ wide-angle x-ray diffraction study. *Macromolecules* **2001**, *34* (17), 5902−5909.
(13) Somani, R. H.; Yang, L.; Zhu, L.; Hsiao, B. S. Flow-induced shish-kebab precursor structures in entangled polymer melts. *Polymer* **2005**, *46* (20), 8587−8623. To Honor the Memory of John D. Hoffman.
(14) Janeschitz-Kriegl, H.; Ratajski, E.; Stadlbauer, M. Flow as an effective promotor of nucleation in polymer melts: a quantitative evaluation. *Rheol. Acta* **2003**, *42* (4), 355−364.
(15) Kumaraswamy, G.; Issaian, A. M.; Kornfield, J. A. Shear-enhanced crystallization in isotactic polypropylene. 1. correspondence between in situ rheo-optics and ex situ structure determination. *Macromolecules* **1999**, *32* (22), 7537−7547.
(16) Seki, M.; Thurman, D. W.; Oberhauser, J. P.; Kornfield, J. A. Shear-mediated crystallization of isotactic polypropylene: The role of long chain-long chain overlap. *Macromolecules* **2002**, *35* (7), 2583−2594.
(17) Balzano, L.; Ma, Z.; Cavallo, D.; Van Erp, T. B.; Fernandez-Ballester, L.; Peters, G. W. M. Molecular aspects of the formation of shish-kebab in isotactic polypropylene. *Macromolecules* **2016**, *49* (10), 3799−3809.
(18) Liedauer, S.; Eder, G.; Janeschitz-Kriegl, H.; Jerschow, P.; Geymayer, W.; Ingolic, E. On the kinetics of shear induced crystallization in polypropylene. *Int. Polym. Process.* **1993**, *8*, 236−244.
(19) Mezghani, K.; Phillips, P. J. The γ-phase of high molecular weight isotactic polypropylene. ii: the morphology of the γ-form crystallized at 200 mpa. *Polymer* **1997**, *38*, 5725−5733.
(20) Mezghani, K.; Phillips, P. J. The γ-phase of high molecular weight isotactic polypropylene. iii: the equilibrium melting point and the phase diagram. *Polymer* **1998**, *39*, 3735−3744.
(21) Angelloz, C.; Fulchiron, R.; Douillard, A.; Chabert, B.; Fillit, R.; Vautrin, A.; David, L. Crystallization of isotactic polypropylene under high pressure: γ-phase. *Macromolecules* **2000**, *33* (1), 4138−4145.
(22) Van Der Beek, M. H. E.; Peters, G. W. M.; Meijer, H. E. H. A dilatometer to measure the influence of cooling rate and melt shearing on specific volume. *Int. Polym. Process.* **2005**, *20* (2), 111−120.
(23) van Erp, T. B.; Balzano, L.; Spoelstra, A. B.; Govaert, L. E.; Peters, G. W. M. Quantification of non-isothermal, multi-phase crystallization of isotactic polypropylene: The influence of shear and pressure. *Polymer* **2012**, *53* (25), 5896−5908.
(24) van Erp, T. B.; Roozemond, P. C.; Peters, G. W. M. Flow-enhanced crystallization kinetics of ipp during cooling at elevated pressure: Characterization, validation, and development. *Macromol. Theory Simul.* **2013**, *22* (5), 309−318.
(25) Yang, S.; Zhang, Z.; Zhang, L.; Zhou, D.; Wang, Y.; Lei, J.; Li, L.; Li, Z. Unexpected shear dependence of pressure-induced [gamma]-crystals in isotactic polypropylene. *Polym. Chem.* **2015**, *6*, 4588−4596.
(26) Lotz, B.; Graff, S.; Wittmann, J. C. Crystal morphology of the γ (triclinic) phase of isotactic polypropylene and its relation to the α phase. *J. Polym. Sci., Part B: Polym. Phys.* **1986**, *24* (9), 2017−2032.
(27) Valdo Meille, S.; Brückner, S. Non-parallel chains in crystalline γ-isotactic polypropylene. *Nature* **1989**, *340* (6233), 455−457.
(28) Roozemond, P. C.; van Erp, T. B.; Peters, G. W. M. Flow-induced crystallization of isotactic polypropylene: Modeling formation of multiple crystal phases and morphologies. *Polymer* **2016**, *89*, 69−80.
(29) Housmans, J. W.; Steenbakkers, R. J. A.; Roozemond, P. C.; Peters, G. W. M.; Meijer, H. E. H. Saturation of pointlike nuclei and the transition to oriented structures in flow-induced crystallization of isotactic polypropylene. *Macromolecules* **2009**, *42* (15), 5728−5740.
(30) van Drongelen, M.; van Erp, T. B.; Peters, G. W. M. Quantification of non-isothermal, multi-phase crystallization of isotactic polypropylene: The influence of cooling rate and pressure. *Polymer* **2012**, *53* (21), 4758−4769.
(31) Housmans, J. W.; Balzano, L.; Santoro, D.; Peters, G. W. M.; Meijer, H. E. H. A design to study flow induced crystallization in a multipass rheometer. *Int. Polym. Process.* **2009**, *24*, 185−197.
(32) Portale, G.; Cavallo, D.; Carlo Alfonso, G.; Hermida-Merino, D.; van Drongelen, M.; Balzano, L.; Peters, G. W. M.; Goossens, J. G. P.; Bras, W. Polymer crystallization studies under processing-relevant conditions at the SAXS/WAXS DUBBLE beamline at the ESRF. *J. Appl. Crystallogr.* **2013**, *46* (6), 1681−1689.
(33) Dean, D. M.; Register, R. A. Oriented γ-isotactic polypropylene crystallized at atmospheric pressure. *J. Polym. Sci., Part B: Polym. Phys.* **1998**, *36* (15), 2821−2827.
(34) Auriemma, F.; De Rosa, C. Crystallization of metallocene-made isotactic polypropylene: Disordered modifications intermediate between the α and γ forms. *Macromolecules* **2002**, *35* (24), 9057−9068.
(35) Auriemma, F.; De Rosa, C. Stretching isotactic polypropylene: From "cross-β" to crosshatches, from γ form to α form. *Macromolecules* **2006**, *39* (22), 7635−7647.
(36) Jones, A. T.; Aizlewood, J. M.; Beckett, D. R. Crystalline forms of isotactic polypropylene. *Makromol. Chem.* **1964**, *75* (1), 134−158.
(37) Murthy, N. S.; Minor, H. General procedure for evaluating amorphous scattering and crystallinity from x-ray diffraction scans of semicrystalline polymers. *Polymer* **1990**, *31* (6), 996−1002.
(38) Roozemond, P. C.; van Drongelen, M.; Ma, Z.; Spoelstra, A. B.; Hermida-Merino, D.; Peters, G. W. M. Self-regulation in flow-induced structure formation of polypropylene. *Macromol. Rapid Commun.* **2015**, *36* (4), 385−390.
(39) Roozemond, P. C.; van Drongelen, M.; Ma, Z.; Hulsen, M. A.; Peters, G. W. M. Modeling flow-induced crystallization in isotactic polypropylene at high shear rates. *J. Rheol.* **2015**, *59* (3), 613−642.
(40) Hatzikiriakos, S. G.; Dealy, J. M. Start-up pressure transients in a capillary rheometer. *Polym. Eng. Sci.* **1994**, *34* (6), 493−499.
(41) Cardinaels, R.; Van Puyvelde, P.; Moldenaers, P. Evaluation and comparison of routes to obtain pressure coefficients from high-pressure capillary rheometry data. *Rheol. Acta* **2007**, *46* (4), 495−505.
(42) Kadijk, S. E.; Van Den Brule, B. H. A. A. On the pressure dependency of the viscosity of molten polymers. *Polym. Eng. Sci.* **1994**, *34* (20), 1535−1546.
(43) van Meerveld, J.; Peters, G. W. M.; Hütter, M. Towards a rheological classification of flow induced crystallization experiments of polymer melts. *Rheol. Acta* **2004**, *44* (2), 119−134.
(44) Somani, R. H.; Hsiao, B. S.; Nogales, A.; Srinivas, S.; Tsou, A. H.; Sics, I.; Balta-Calleja, F. J.; Ezquerra, T. A. Structure development during shear flow-induced crystallization of i-pp: In-situ small-angle x-ray scattering study. *Macromolecules* **2000**, *33* (25), 9385−9394.

DOI: 10.1021/acs.macromol.7b00595
Macromolecules 2017, 50, 3868−3882

(45) Lagasse, R. R.; Maxwell, B. An experimental study of the kinetics of polymer crystallization during shear flow. *Polym. Eng. Sci.* **1976**, *16* (3), 189−199.
(46) Jerschow, P.; Janeschitz-Kriegl, H. The role of long molecules and nucleating agents in shear induced crystallization of isotactic polypropylenes. *Int. Polym. Process.* **1997**, *12* (1), 72−77.
(47) Vleeshouwers, S.; Meijer, H. E. H. A rheological study of shear induced crystallization. *Rheol. Acta* **1996**, *35* (5), 391−399.
(48) Kimata, S.; Sakurai, T.; Nozue, Y.; Kasahara, T.; Yamaguchi, N.; Karino, T.; Shibayama, M.; Kornfield, J. A. Molecular basis of the shish-kebab morphology in polymer crystallization. *Science* **2007**, *316* (5827), 1014−1017.
(49) Ma, Z.; Balzano, L.; van Erp, T.; Portale, G.; Peters, G. W. M. Short-term flow induced crystallization in isotactic polypropylene: How short is short? *Macromolecules* **2013**, *46* (23), 9249−9258.
(50) Verbeeten, W. M. H.; Peters, G. W. M.; Baaijens, F. P. T. Differential constitutive equations for polymer melts: The extended pom-pom model. *J. Rheol.* **2001**, *45* (4), 823−843.
(51) van Drongelen, M.; Roozemond, P. C.; Troisi, E. M.; Doufas, A. K.; Peters, G. W. M. Characterization of the primary and secondary crystallization kinetics of a linear low-density polyethylene in quiescent- and flow-conditions. *Polymer* **2015**, *76*, 254−270.
(52) Macosko, C. W. *Rheology, Principles, Measurements and Application*; Wiley-VCH: New York, 1994.
(53) Vega, J. F.; Rastogi, S.; Peters, G. W. M.; Meijer, H. E. H. Rheology and reptation of linear polymers. ultrahigh molecular weight chain dynamics in the melt. *J. Rheol.* **2004**, *48* (3), 663−678.
(54) Balzano, L.; Kukalyekar, N.; Rastogi, S.; Peters, G. W. M.; Chadwick, J. C. Crystallization and dissolution of flow-induced precursors. *Phys. Rev. Lett.* **2008**, *100*, 048302.
(55) Fernandez-Ballester, L.; Thurman, D. W.; Zhou, W.; Kornfield, J. A. Effect of long chains on the threshold stresses for flow-induced crystallization in ipp: Shish kebabs vs sausages. *Macromolecules* **2012**, *45* (16), 6557−6570.
(56) Leugering, V. H. J. Einfluß der kristallstruktur und der überstruktur auf einige eigenschaften von polypropylen. *Makromol. Chem.* **1967**, *109* (1), 204−216.
(57) Varga, J.; Mudra, I.; Ehrenstein, G. W. Highly active thermally stable β-nucleating agents for isotactic polypropylene. *J. Appl. Polym. Sci.* **1999**, *74* (10), 2357−2368.
(58) Mathieu, C.; Thierry, A.; Wittmann, J. C.; Lotz, B. Specificity and versatility of nucleating agents toward isotactic polypropylene crystal phases. *J. Polym. Sci., Part B: Polym. Phys.* **2002**, *40* (22), 2504−2515.
(59) Varga, J.; Karger-Kocsis, J. Rules of supermolecular structure formation in sheared isotactic polypropylene melts. *J. Polym. Sci., Part B: Polym. Phys.* **1996**, *34* (4), 657−670.
(60) Kumaraswamy, G.; Verma, R. K.; Kornfield, J. A.; Yeh, F.; Hsiao, B. S. Shear-enhanced crystallization in isotactic polypropylene. in-situ synchrotron saxs and waxd. *Macromolecules* **2004**, *37* (24), 9005−9017.
(61) Roozemond, P. C.; Ma, Z.; Cui, K.; Li, L.; Peters, G. W. M. Multimorphological crystallization of shish-kebab structures in isotactic polypropylene: Quantitative modeling of parent-daughter crystallization kinetics. *Macromolecules* **2014**, *47* (15), 5152−5162.

DOI: 10.1021/acs.macromol.7b00595
Macromolecules 2017, 50, 3868−3882